CHEMISTRY
A EUROPEAN JOURNAL

FULL PAPER

DOI: 10.1002/chem.201301641

Mononuclear Manganese–Peroxo and Bis(μ-oxo)dimanganese Complexes Bearing a Common N-Methylated Macrocyclic Ligand

Hyeona Kang,[a] Jaeheung Cho,*[b] Kyung-Bin Cho,[a] Takashi Nomura,[c] Takashi Ogura,[c] and Wonwoo Nam*[a]

Abstract: Mononuclear Mn^{III}–peroxo and dinuclear bis(μ-oxo)Mn^{III}_2 complexes that bear a common macrocyclic ligand were synthesized by controlling the concentration of the starting Mn^{II} complex in the reaction of H_2O_2 (i.e., a Mn^{III}–peroxo complex at a low concentration ($\leq$1 mM) and a bis(μ-oxo)Mn^{III}_2 complex at a high concentration ($\geq$30 mM)). These intermediates were successfully characterized by various physicochemical methods such as UV–visible spectroscopy, ESI-MS, resonance Raman, and X-ray analysis. The structural and spectroscopic characterization combined with density functional theory (DFT) calculations demonstrated unambiguously that the peroxo ligand is bound in a side-on fashion in the Mn^{III}–peroxo complex and the Mn_2O_2 diamond core is in the bis(μ-oxo)Mn^{III}_2 complex. The reactivity of these intermediates was investigated in electrophilic and nucleophilic reactions, in which only the Mn^{III}–peroxo complex showed a nucleophilic reactivity in the deformylation of aldehydes.

Keywords: aldehyde deformylation · bioinorganic chemistry · kinetics · manganese · peroxo ligands

Introduction

Metal–oxygen adducts (M_x–O_x, $x=1$ or 2), such as metal–superoxo, –peroxo, and –oxo species, are key intermediates often detected in the catalytic cycles of dioxygen activation by metalloenzymes.[1] In biomimetic and synthetic chemistry, numerous M_x–O_x complexes have been prepared and characterized with various physicochemical methods as structural and functional models of enzymes.[2] Among the M_x–O_2 adducts, manganese–oxygen species (Mn_x–O_2) have attracted much attention, since the intermediates have been invoked as reactive species in Mn-containing enzymes such as catalase, superoxide dismutase, and the oxygen-evolving complex (OEC) of photosystem II.[3] Recent advances in synthetic model chemistry have provided fundamental information on the structures and chemical properties of Mn_x–O_2 species.[4,5] For example, a number of bis(μ-oxo)Mn^{III}_2 complexes have been synthesized and investigated in water exchange, oxidation reaction, and redox chemistry to understand the OEC.[3,5] We have also reported the synthesis, characterization, and reactivity of Mn^{III}–peroxo complexes that bear N-methylated cyclam ligands, $[Mn^{III}(13\text{-TMC})(O_2)]^+$ and $[Mn^{III}(14\text{-TMC})(O_2)]^+$ (Scheme 1)[6] and

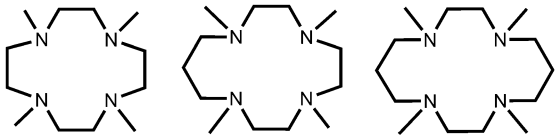

Scheme 1. A schematic drawing of *n*-TMC ($n=12$, 13, 14) ligands.

we have highlighted a notable axial ligand effect on the reactivity of the Mn^{III}–peroxo species.[7] Our recent account has shown the importance of metal ions and supporting ligands in tuning the electronic and geometric structures and reactivity of various metal–O_2 intermediates including Mn–O_2 species.[8] However, to the best of our knowledge, the reactivity of bis(μ-oxo)Mn^{III}_2 and Mn^{III}–peroxo complexes that bear the same supporting ligand has never been compared directly, although mononuclear Ni^{II}–superoxo and Ni^{III}–peroxo complexes that bear a common macrocyclic ligand were reported very recently.[9] Herein we report synthetic routes to the formation of two different Mn_x–O_2 complexes that bear a common 12-TMC[6] ligand ($x=1$ for a mononuclear Mn^{III}–peroxo complex; $x=2$ for a bis(μ-oxo)Mn^{III}_2 complex). The intermediates were characterized by means of various spectroscopic methods and X-ray crystallography combined with density functional theory (DFT) calcula-

[a] H. Kang, Dr. K.-B. Cho, Prof. Dr. W. Nam
Department of Bioinspired Science
Department of Chemistry and Nano Science
Ewha Womans University, Seoul 120-750 (Korea)
E-mail: wwnam@ewha.ac.kr

[b] Prof. Dr. J. Cho
Department of Emerging Materials Science
DGIST, Daegu 711-873 (Korea)
E-mail: jaeheung@dgist.ac.kr

[c] T. Nomura, Prof. Dr. T. Ogura
Picobiology Institute, Graduate School of Life Science
University of Hyogo, Koto 3-2-1, Kamigori-cho
Ako-gun, Hyogo 678-1297 (Japan)

Supporting information for this article is available on the WWW under http://dx.doi.org/10.1002/chem.201301641.

tions.[10] In addition, the Mn_x–O_2 intermediates have been employed in investigating their reactivities in nucleophilic and electrophilic reactions.

Results and Discussion

Synthetic procedures for Mn^{III}–peroxo and bis(μ-oxo)Mn^{III}_2 complexes are illustrated in Scheme 2. The starting Mn^{II}

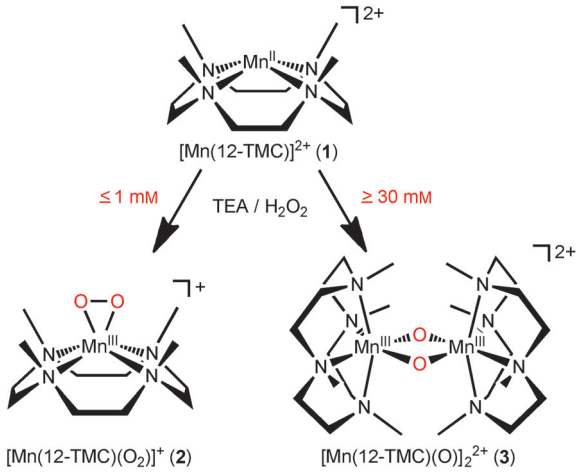

Scheme 2. Synthetic procedures for mononuclear Mn^{III}–peroxo (**2**) and dinuclear bis(μ-oxo)Mn^{III}_2 (**3**) complexes.

complex, $[Mn^{II}(12\text{-TMC})]^{2+}$ (**1**), was prepared by reacting equimolar amounts of $Mn^{II}(OTf)_2$ ($OTf = CF_3SO_3^-$) and 12-TMC in CH_3CN, followed by characterization with UV–visible absorption spectroscopy (Figure 1a) and electrospray ionization mass spectrometry (ESI-MS; Figure S1 in the Supporting Information). Then, a Mn^{III}–peroxo complex, $[Mn^{III}(12\text{-TMC})(O_2)]^+$ (**2**), was synthesized by adding H_2O_2 (5 equiv) to a solution of **1** in CF_3CH_2OH (1 mM) that contained triethylamine (TEA; 2 equiv) at 20 °C; the color of the solution changed to yellowish green (Scheme 2). The UV–visible spectrum of **2** shows an intense band at 280 nm ($\varepsilon = 2600\ M^{-1}cm^{-1}$) and two weak bands at 455 ($\varepsilon = 250\ M^{-1}cm^{-1}$) and 620 nm ($\varepsilon = 200\ M^{-1}cm^{-1}$; Figure 1a), similar to those of the previously reported Mn^{III}–peroxo complexes that bear 13-TMC and 14-TMC ligands, $[Mn^{III}(13\text{-TMC})(O_2)]^+$ and $[Mn^{III}(14\text{-TMC})(O_2)]^+$, respectively.[7] Such absorption bands have also been observed in six-coordinate side-on Mn^{III}–peroxo complexes supported by pentadentate ligands and have been assigned to a peroxo-to-manganese(III) charge-transfer (CT) transition and d–d transitions.[11] The ESI-MS of **2** exhibits a prominent ion peak at a mass-to-charge ratio (m/z) of 315.1 (Figure 1b), and the mass and isotope distribution pattern correspond to $[Mn(12\text{-TMC})(O_2)]^+$ (calculated m/z of 315.2). When the reaction was carried out with isotopically labeled $H_2{}^{18}O_2$, a mass peak that corresponds to $[Mn(12\text{-TMC})(^{18}O_2)]^+$ appeared at m/z of 319.1 (calculated m/z of 319.2; Figure 1b, inset). The

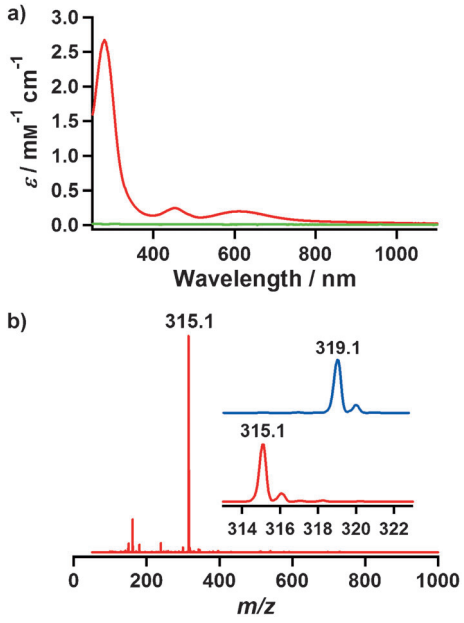

Figure 1. a) UV–visible spectra of $[Mn^{II}(12\text{-TMC})]^{2+}$ (**1**; green line) and $[Mn^{III}(12\text{-TMC})(O_2)]^+$ (**2**; red line) in CF_3CH_2OH at 20 °C. b) ESI-MS of **2** in CF_3CH_2OH at 20 °C. Insets: the observed isotope distribution patterns for $[Mn^{III}(12\text{-TMC})(^{16}O_2)]^+$ (bottom) and $[Mn^{III}(12\text{-TMC})(^{18}O_2)]^+$ (top).

shift in four mass units upon substitution of ^{16}O with ^{18}O proves that **2** contains an O_2 unit.

Single crystals of **2**-(ClO_4) contained two crystallographically independent but virtually identical cations in the asymmetric unit (denoted "A" and "B"; Tables S1 and S2 in the Supporting Information). The X-ray crystal structure of **2**-(ClO_4) revealed the mononuclear side-on 1:1 manganese complex of O_2 in a distorted-octahedral geometry that arises from the triangular MnO_2 moiety with a small bite angle of 44.7° (Figure 2a). The O–O bond of 1.408 Å is typical of a peroxo group bound to a transition-metal ion[12] and it is comparable to those of $[Mn^{III}(13\text{-TMC})(O_2)]^+$ (1.410 Å) and $[Mn^{III}(14\text{-TMC})(O_2)]^+$ (1.403 Å; Table 1).[7] The peroxo

Table 1. Structural comparison for MnO_2 moieties [Å] in $[Mn^{III}(12\text{-TMC})(O_2)]^+$ (**2**), $[Mn^{III}(13\text{-TMC})(O_2)]^+$, and $[Mn^{III}(14\text{-TMC})(O_2)]^+$.

	$[Mn^{III}(12\text{-TMC})(O_2)]^+$ (**2**)	$[Mn^{III}(13\text{-TMC})(O_2)]^+$[a]	$[Mn^{III}(14\text{-TMC})(O_2)]^+$[b]
$Mn\cdots 4N_{plane}$	0.771[c]	0.6734	0.5679
O–O	1.408[c]	1.410	1.403
Mn–O	1.853[c]	1.859[c]	1.884[c]

[a] Ref. [7a]. [b] Ref. [7b]. [c] Averaged data.

group is symmetrically bound to the manganese center in a side-on fashion with an average Mn–O bond of 1.853 Å, which is also comparable to those of $[Mn^{III}(13\text{-TMC})(O_2)]^+$ (1.859 Å) and $[Mn^{III}(14\text{-TMC})(O_2)]^+$ (1.884 Å). All four N-methyl groups of the 12-TMC ligand are oriented *syn* to the peroxo group, as observed in other metal(III)–peroxo complexes that bear macrocyclic N-tetramethylated cyclam li-

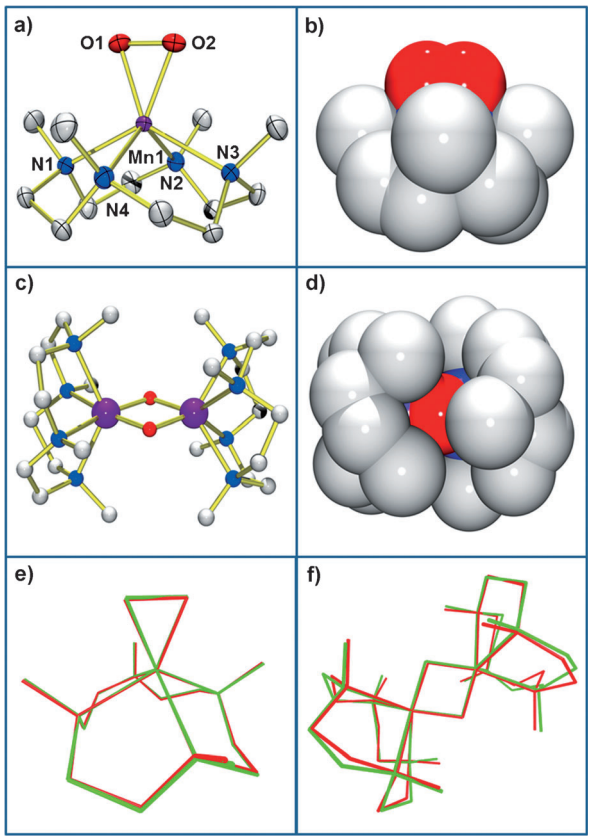

Figure 2. Structures of $[Mn^{III}(12\text{-}TMC)(O_2)]^+$ (**2**) and $[Mn^{III}(12\text{-}TMC)(O)]_2^{2+}$ (**3**). Hydrogen atoms are omitted for clarity. a) ORTEP plot of **2A** with 30% probability thermal ellipsoid. Some average bond lengths [Å] and angles [°]: Mn–O 1.853, O–O 1.408; O–Mn–O 44.7. b) Space-filling representation of **2**. c) Ball-and-stick, and d) space-filling representation of a preliminary X-ray structure for **3**. Overlap of the crystal (red) and the DFT-calculated (green) structures for: e) **2**, and f) **3**.

gands.[8,13] In addition, it is noteworthy that the ring size of the supporting ligands does not affect the MnO_2 core (Table 1). However, a significant difference was observed in the distance between the Mn^{III} center and 4N plane (0.771 Å for **2**; 0.6734 Å for $[Mn^{III}(13\text{-}TMC)(O_2)]^+$; 0.5679 Å for $[Mn^{III}(14\text{-}TMC)(O_2)]^+$), whereby the 4N plane is defined by the mean plane of the four N atoms from the macrocyclic ligands. The distances of the MnO_2 moiety from the 4N plane are found to increase as the ring size of the supporting ligands becomes smaller (Figure S2 in the Supporting Information).

DFT calculations were also carried out on **2**, and the calculated structure could be compared to the crystal structure to gauge the reliability of the calculations. These comparisons indicate that the deviation on the Mn–O distance is 0.01 Å, whereas the O–O bond difference is slightly larger: 0.03 Å (Table 1 and Table S2 in the Supporting Information). Figure 2e shows an overlap of the structures aligned at the MnO_2 moiety, which show an acceptable agreement with a root-mean-square deviation (RMSD) of 0.03 Å. Mulliken spin-density distribution analysis shows 3.92 in the spin density on Mn and −0.02 on each of the two oxygen atoms, as expected from a $S=2$ Mn^{III}–peroxo species. Our conclusion from these results is that DFT at the employed level reproduces the experimental results and can give credible results for our $Mn_2(\mu\text{-}O)_2$ systems (see below).

Interestingly, when **1** in a high-concentration solution (e.g., ≥30 mM) was treated with H_2O_2 (5 equiv) in the presence of TEA (2 equiv) in CF_3CH_2OH at 20 °C, a different intermediate was isolated from the olive green solution in good yield (69%; Scheme 2).[14] This complex was identified as $[Mn^{III}(12\text{-}TMC)(O)]_2^{2+}$ (**3**) on the basis of UV–visible spectroscopy, ESI-MS, and resonance Raman measurements and a preliminary X-ray crystal structure analysis (Figure 2c).[15] In the UV–visible spectrum, an intense band at 320 nm ($\varepsilon=860\,M^{-1}cm^{-1}$) and two weak bands at 415 ($\varepsilon=320\,M^{-1}cm^{-1}$) and 600 nm ($\varepsilon=200\,M^{-1}cm^{-1}$) were observed (Figure 3a); the latter band was assigned as a d–d transition

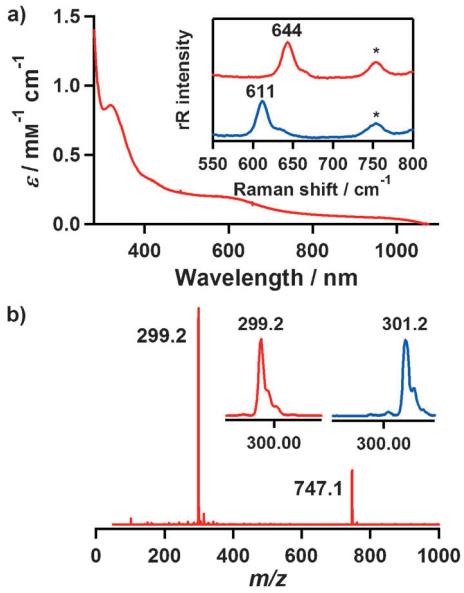

Figure 3. a) UV–visible spectrum of $[Mn^{III}(12\text{-}TMC)(O)]_2^{2+}$ (**3**) in CF_3CH_2OH at 20 °C. Inset: resonance Raman spectra of **3** prepared with $H_2{}^{16}O_2$ (red line) and $H_2{}^{18}O_2$ (blue line). The solvent peak is marked with an asterisk. b) ESI-MS of **3** in CF_3CH_2OH at 20 °C. Mass peaks m/z 299.2 and 747.1 are assigned to $\{[Mn^{III}(12\text{-}TMC)(O)]_2\}^{2+}$ and $\{[Mn^{III}(12\text{-}TMC)(O)]_2(OTf)\}^+$, respectively. Insets: the observed isotope distribution patterns for $[Mn^{III}(12\text{-}TMC)(^{16}O)]_2^{2+}$ (red line) and $[Mn^{III}(12\text{-}TMC)(^{18}O)]_2^{2+}$ (blue line).

by analogy to similar data reported for bis(μ-oxo)Mn^{III}_2 complexes.[5,16] When the resonance Raman spectrum of **3** was collected using 364 nm excitation in CH_3CN at −20 °C, **3** prepared with $H_2{}^{16}O_2$ exhibits an isotopically sensitive band at 644 cm^{-1} that shifts to 611 cm^{-1} in a sample prepared with $H_2{}^{18}O_2$ (Figure 3a, inset). The band can be assigned to the symmetric breathing mode of a Mn_2O_2 core, as reported in bis(μ-oxo)dimetal(III) complexes of nickel and copper (≈600 cm^{-1}).[17,18] The ESI-MS of **3** shows major peaks at m/z 299.2 and 747.1 (Figure 3b), and the mass and isotope distribution patterns correspond to $\{[Mn^{III}(12\text{-}TMC)(O)]_2\}^{2+}$ and $\{[Mn^{III}(12\text{-}TMC)(O)]_2(OTf)\}^+$, respec-

tively. When the reaction was carried out with isotopically labeled $H_2{}^{18}O_2$, a mass peak that corresponds to $\{[Mn^{III}(12\text{-}TMC)(^{18}O)]_2\}^{2+}$ appeared at m/z 301.2 (calcd m/z 301.2; Figure 3b, inset), thus indicating that **3** contains two oxygen atoms. The X-ray structure of **3** shows a dinuclear structure with a $Mn_2(\mu\text{-}O)_2$ moiety, but the average Mn–O (1.817 Å) and Mn···Mn (2.7676(19) Å) distances are not reliable owing to severe disorder problems. Nevertheless, these values are comparable to those observed in other bis(μ-oxo)Mn^{III}_2 complexes.[5,16,19]

Since the crystal structure suffers from disorder problems, it is interesting to compare this to the DFT-calculated structure for this species. Figure 2f shows an overlap of the crystal structure of **3** and the DFT-calculated structure. It can be seen that the $Mn_2(\mu\text{-}O)_2$ core itself is well aligned, whereas slightly differing Mn–N distances affect the overlap positions of the ligand. However, with an RMSD of 0.11 Å, the agreement must still be regarded as quite good despite the disorder in the crystal structure. One should also remember that the calculations are done in the solvent state, which is presumably slightly different from the crystal structure in crystallographic conditions.

The reactivity of **2** and **3** was investigated in nucleophilic and electrophilic reactions. First, the nucleophilic character of **2** was tested in aldehyde deformylation with 2-phenylpropionaldehyde (2-PPA). Upon addition of 2-PPA to **2** in CF_3CH_2OH at 20°C, the characteristic UV–visible absorption bands of **2** disappeared with a pseudo-first-order decay profile (Figure 4a). The pseudo-first-order rate constants increased proportionally along with the 2-PPA concentration ($k_2 = 4.4\times10^{-2}\,M^{-1}s^{-1}$; Figure 4b). Product analysis of the reaction mixture with GC/GC-MS revealed the formation of acetophenone (90(±10)%). Activation parameters for the aldehyde deformylation of **2** between 288 and 303 K were determined to be $\Delta H^{\neq} = 88\,kJ\,mol^{-1}$ and $\Delta S^{\neq} = -57\,J\,mol^{-1}K^{-1}$ (Figure 4c). It is of interest to compare the reactivity of **2** in aldehyde deformylation with that of previously reported Mn^{III}–peroxo complexes with different ring sizes of *n*-TMC ($n = 12$, 13, 14). The rate of aldehyde deformylation of $[Mn^{III}(13\text{-}TMC)(O_2)]^+$ and $[Mn^{III}(14\text{-}TMC)(O_2)]^+$ in CF_3CH_2OH at 20°C were further determined as a function of 2-PPA concentration under identical reaction conditions (Table 2). The reactivity of **2** ($k_2 = 4.4\times10^{-2}\,M^{-1}s^{-1}$) is similar to that of $[Mn^{III}(13\text{-}TMC)(O_2)]^+$ ($k_2 = 2.9\times10^{-2}\,M^{-1}s^{-1}$) and $[Mn^{III}(14\text{-}TMC)(O_2)]^+$ ($k_2 = 4.3\times10^{-2}\,M^{-1}s^{-1}$) in the deformylation of 2-PPA, thus indicating that the nucleophilicity of Mn^{III}–peroxo complexes does not change significantly depending on the ring size of the supporting ligands. These results can be understood by considering the relationship between the MnO_2 core geometry and the ring size of the supporting ligands (see above, Table 1). One can also make the argument that in Mn^{III}–peroxo species, the valence orbital is likely to be the most affected by the ligand ring size is σ^*_{xy} (Figure S3 in the Supporting Information). This is because it is the only one of the valence orbitals that is delocalized over the ligand atoms. In a deformylation reaction at high-spin state, this orbital is singly occupied from start to finish and hence does not participate in the reaction. Therefore, the reaction activation energy should be more or less independent of the energy of this orbital; hence, no large energy shifts due to the ligand size are expected.

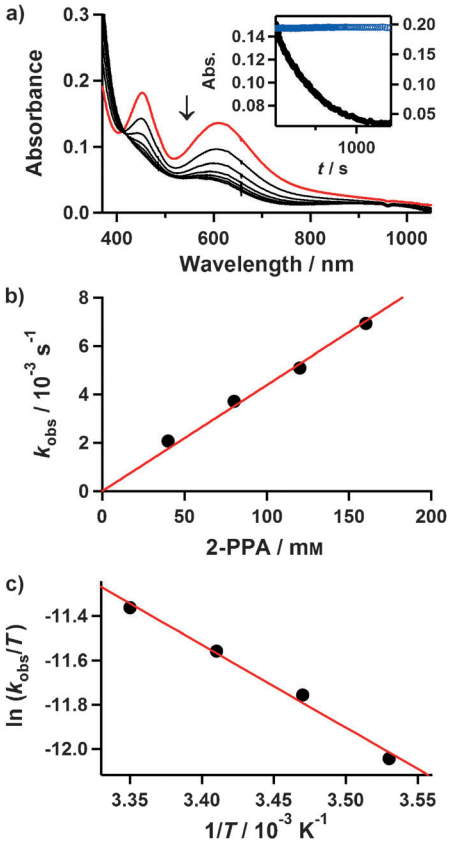

Figure 4. Reactions of $[Mn(12\text{-}TMC)(O_2)]^+$ (**2**) with 2-PPA in CF_3CH_2OH at 20°C. a) UV–visible spectral changes of **2** (1 mM) upon addition of 2-PPA (20 equiv). Inset: the time course of the absorbance at 610 nm for **2** (black circles, left axis) and $[Mn(12\text{-}TMC)(O)]_2^{2+}$ (**3**; blue circles, right axis). b) Plot of k_{obs} against 2-PPA concentration to determine a second-order rate constant. c) Plot of first-order rate constants against $1/T$ to determine activation parameters for the reaction of **2** (1 mM) and 2-PPA (20 equiv).

Table 2. Kinetic data for aldehyde deformylation of $[Mn^{III}(12\text{-}TMC)(O_2)]^+$ (**2**), $[Mn^{III}(13\text{-}TMC)(O_2)]^+$, and $[Mn^{III}(14\text{-}TMC)(O_2)]^+$ in CF_3CH_2OH at 20°C.

Complex	2-PPA (k_2) [$M^{-1}s^{-1}$]	Yield [%]
$[Mn^{III}(12\text{-}TMC)(O_2)]^+$ (**2**)	4.4×10^{-2}	90±10
$[Mn^{III}(13\text{-}TMC)(O_2)]^+$	2.9×10^{-2}	85±10
$[Mn^{III}(14\text{-}TMC)(O_2)]^+$	4.3×10^{-2}	80±10

In contrast, upon addition of 2-PPA to a solution of **3** in CF_3CH_2OH at 20°C, **3** remained intact without showing any absorption spectral change (Figure 4a, inset), thereby demonstrating that **3** is not capable of conducting the nucleophilic oxidation reaction. The poor reactivity of **3** in aldehyde deformylation might result from the steric encumbrance for the access of external substrates to the $Mn_2(\mu$-

$O)_2$ moiety (Figure 2). The electrophilic character of **2** and **3** was tested in the oxidation of PPh_3 and xanthene. Upon addition of the substrates to **2** and **3** in CF_3CH_2OH at 20 °C, the intermediates remained intact without showing any absorption spectral change, and product analysis of the reaction solutions revealed that no oxygenated products were formed in the reactions. These results demonstrate that **2** and **3** are not capable of conducting an electrophilic oxidation reaction.[20]

Conclusion

We have shown the formation of two different intermediates in the reaction of a manganese complex that bears a 12-TMC ligand and H_2O_2 depending on the concentration of the starting Mn^{II} complex (i.e., a mononuclear Mn^{III}–peroxo complex at a low concentration and a dinuclear bis(μ-oxo)-Mn^{III}_2 complex at a high concentration). DFT-optimized structures agree with the crystal structures with RMSD values of 0.03 and 0.11 Å for **2** and **3**, respectively. The excellent agreement of the former species gives credibility to the DFT-calculated structure of the latter one, which is in good agreement with the crystal structure even as it suffers from severe disorder. In reactivity studies, only the Mn^{III}–peroxo complex showed nucleophilic character in the deformylation of aldehydes.

Experimental Section

Materials: All chemicals obtained from Aldrich Chemical Co. were the best available purity and used without further purification unless otherwise indicated. Solvents were dried according to published procedures and distilled under Ar prior to use.[21] $H_2{}^{18}O_2$ (95% ^{18}O-enriched, 2% $H_2{}^{18}O_2$ in water) was purchased from ICON Services Inc. (Summit, NJ, USA). The 12-TMC was prepared by treating an excess amount of formaldehyde and formic acid with 1,4,7,10-tetraazacyclododecane.[22] $[Mn^{III}(13\text{-TMC})(O_2)]^+$ and $[Mn^{III}(14\text{-TMC})(O_2)]^+$ were prepared according to the literature methods.[7]

Synthesis and characterization of $[Mn^{II}(12\text{-TMC})](OTf)_2$ (1-$(OTf)_2$): 12-TMC (0.5 g, 2.19 mmol) was added to a solution of $Mn^{II}(OTf)_2$ (0.93 g, 2.19 mmol) in acetonitrile (0.5 mL). The mixture was stirred for several hours, and then Et_2O (4 mL) was added to the resulting solution to yield a white powder, which was collected by filtration, washed with Et_2O, and dried under vacuum. Yield: 0.87 g (68%); UV/Vis (CH_3CN): see Figure 1; ESI-MS (CH_3CN; Figure S1 in the Supporting Information): m/z: 162.0 $[Mn(12\text{-TMC})(CH_3CN)]^{2+}$, 432.2 $[Mn(12\text{-TMC})(OTf)]^+$.

Generation and characterization of $[Mn^{III}(12\text{-TMC})(O_2)]^+$ (2): Treatment of **1** (1 mM) with H_2O_2 (5 equiv) in the presence of triethylamine (TEA; 2 equiv) in CF_3CH_2OH (2 mL) afforded the formation of a green solution at 20 °C. Spectroscopic data including UV/Vis and ESI-MS are reported in Figure 1. $[Mn^{III}(12\text{-TMC})(^{18}O_2)]^+$ was prepared by adding $H_2{}^{18}O_2$ (5 equiv; 18 μL, 90% ^{18}O-enriched, 2% $H_2{}^{18}O_2$ in water) in the presence of TEA (2 equiv) in CF_3CH_2OH at 20 °C. X-ray crystallographically suitable crystals were obtained by slow diffusion of Et_2O into a solution of the complex with an excess amount of $NaClO_4$. Caution: Perchlorate salts are potentially explosive and should be handled with care!

Generation and characterization of $[Mn^{III}(12\text{-TMC})(O)]_2{}^{2+}$ (3): Treatment of **1** (50 mM) with H_2O_2 (5 equiv) in the presence of TEA (2 equiv) in CF_3CH_2OH (1 mL) afforded the formation of an olive green solution at 20 °C. The mixture was stirred for several hours, and then Et_2O (40 mL) was added to the resulting solution to yield a dark green powder, which was collected by filtration, washed with Et_2O, and dried under vacuum. Yield: 0.02 g (69%). Spectroscopic data including UV/Vis, resonance Raman, and ESI-MS are reported in Figure 3. Resonance Raman spectra of **3** were measured in CH_3CN instead of CF_3CH_2OH on account of an overlap with intense solvent bands. $[Mn^{III}(12\text{-TMC})(^{18}O)]_2{}^{2+}$ was prepared by adding $H_2{}^{18}O_2$ (5 equiv; 525 μL, 90% ^{18}O-enriched, 2% $H_2{}^{18}O_2$ in water) to a solution that contained **1** (30 mM) and TEA (2 equiv) in CF_3CH_2OH (2 mL) at ambient temperature.

Instrumentation: UV/Vis spectra were recorded using a Hewlett Packard 8453 diode array spectrophotometer equipped with a UNISOKU Scientific Instruments for low-temperature experiments or with a circulating water bath. Electrospray ionization mass spectra were collected using a Thermo Finnigan (San Jose, CA, USA) LCQ Advantage MAX quadrupole ion-trap instrument, by infusing samples directly into the source using a manual method. The spray voltage was set at 4.2 kV and the capillary temperature at 80 °C. Resonance Raman spectra were obtained using a liquid-nitrogen-cooled CCD detector (Symphony 1024×256, HORIBA) attached to a 1 m single polychromator (MC-100DG, Ritsu Oyo Kogaku) with a 1200 grooves mm^{-1} holographic grating. An excitation wavelength of 363.8 nm was provided by an Ar^+ laser (Spectra Physics, BeamLok 2080) with 20 mW power at the sample point. All measurements were carried out with a spinning cell (400 rpm) at −20 °C. Raman shifts were calibrated with indene, and the accuracy of the peak positions of the Raman bands was ±1 cm^{-1}. Product analysis was performed using an Agilent Technologies 6890N gas chromatograph and Thermo Finnigan (Austin, Texas, USA) FOCUS DSQ (dual stage quadrupole) mass spectrometer interfaced with a Finnigan FOCUS gas chromatograph (GC-MS).

X-ray crystallography: Single crystals of **2**-(ClO_4) were picked from solutions by a nylon loop (Hampton Research Co.) on a handmade copper plate mounted inside a liquid N_2 Dewar vessel at approximately −40 °C and mounted on a goniometer head in a N_2 cryostream. Data collections were carried out using a Bruker SMART APEX II CCD diffractometer equipped with a monochromator in the $Mo_{K\alpha}$ (λ=0.71073 Å) incident beam. The CCD data were integrated and scaled using the Bruker-SAINT software package, and the structure was solved and refined using SHELXTL V6.12.[23] Compound **2**-(ClO_4) crystallized with two crystallographically independent but virtually identical cations in the asymmetric unit (denoted "A" and "B"). Two oxygen atoms in **2A** and **2B** were found to be disordered over two positions. Hydrogen atoms were located in the calculated positions for **2**-(ClO_4).

Crystal data for **2**-(ClO_4): $C_{12}H_{28}ClMnN_4O_6$; monoclinic, *P21/n*; Z=8; a=21.9331(6), b=7.6475(2), c=22.3583(6) Å; β=98.958(2)°; V=3704.49(17) $Å^3$; μ=0.891 mm^{-1}; ρ_{calcd}=1.487 $g\,cm^{-3}$; R_1=0.0531, wR_2=0.1534 for 7291 unique reflections, 477 variables. The crystallographic data for **2**-(ClO_4) are listed in Table S1 of the Supporting Information, and Table S2 of the Supporting Information lists the selected bond lengths and angles.

CCDC-914131 (**2**-(ClO_4)) contains the supplementary crystallographic data for this paper. These data can be obtained free of charge from The Cambridge Crystallographic Data Centre via www.ccdc.cam.ac.uk/data_request/cif.

DFT calculations: Calculations were carried out with the BP86 functional.[24] Although there are other functionals that are considered superior in giving accurate energies (i.e., B3LYP), this functional is known to give fairly good geometrical structures that many times surpass B3LYP. As our main concern here is structural parameters rather than energies, this functional was deemed to fit our purposes better. The basis set used was TZVP[25] (except on Mn) using the ORCA[26] program. Mn atoms used a triply polarized core-properties basis set CP(PPP)[27] as defined in ORCA, with an enhanced integration grid in which the overall integration accuracy was increased to 7. Solvent (acetonitrile) effects were modeled with the COSMO scheme[28] and was included in the optimizations. The RMSD values were calculated using VMD.[29]

Kinetic measurements: All reactions were run by monitoring UV/Vis spectral changes of reaction solutions, and rate constants were determined by fitting the changes in absorbance at 610 nm for $[Mn^{III}(12\text{-}$

TMC)$(O_2)]^+$ (**2**) and 600 nm for $[Mn^{III}(12\text{-TMC})(O)]_2^{2+}$ (**3**). Reactions were run at least in triplicate, and the data reported represent the average of these reactions. In situ generated **2** and **3** were used in kinetic studies. After the completion of reactions, pseudo-first-order fitting of the kinetic data allowed us to determine k_{obs} values. Products formed in the oxidation of 2-phenylpropionaldehyde (2-PPA) by **2** in CF_3CH_2OH at 20 °C were analyzed by GC and GC-MS. The purity of substrates was checked with GC and GC-MS prior to use. Products were analyzed by injecting the reaction mixture directly into GC and GC-MS devices. Products were identified by comparison with authentic samples, and product yields were determined by comparison against standard curves prepared with authentic samples and using decane as an internal standard.

Acknowledgements

W.N. at EWU acknowledges the financial support from the NRF/MEST of Korea through the CRI (2-2012-1794-001-1), GRL (2010-00353), and WCU (R31-2008-000-10010-0). J.C. at DGIST acknowledges financial support from the R&D program of the MEST of Korea (13-BD-0403 and 2013K2A2A4000610). Portions of this research were supported by the Ministry of Education, Culture, Sports, Science and Technology of Japan through the Global COE program and Priority Area (no. 20050029; T.O.).

[1] a) P. R. Ortiz de Montellano, *Chem. Rev.* **2010**, *110*, 932–948; b) M. T. Green, *Curr. Opin. Chem. Biol.* **2009**, *13*, 84–88; c) C. Krebs, D. G. Fujimori, C. T. Walsh, J. M. Bollinger, Jr., *Acc. Chem. Res.* **2007**, *40*, 484–492; d) W. Nam, *Acc. Chem. Res.* **2007**, *40*, 465, and review articles in the special issue; e) M. M. Abu-Omar, A. Loaiza, N. Hontzeas, *Chem. Rev.* **2005**, *105*, 2227–2252; f) I. M. Klotz, D. M. Kurtz, Jr., *Chem. Rev.* **1994**, *94*, 567–568, and review articles in the special issue; g) W. B. Tolman, E. I. Solomon, *Inorg. Chem.* **2010**, *49*, 3555–3556; h) A. Gunay, K. H. Theopold, *Chem. Rev.* **2010**, *110*, 1060–1081; i) A. S. Borovik, *Chem. Soc. Rev.* **2011**, *40*, 1870–1874; j) J. M. Mayer, *Acc. Chem. Res.* **2011**, *44*, 36–46; k) J. Hohenberger, K. Ray, K. Meyer, *Nat. Commun.* **2012**, *3*, 720; l) S. P. de Visser, J.-U. Rohde, Y.-M. Lee, J. Cho, W. Nam, *Coord. Chem. Rev.* **2013**, *257*, 381–393.

[2] a) S. Itoh, *Curr. Opin. Chem. Biol.* **2006**, *10*, 115–122; b) C. Würtele, E. Gaoutchenova, K. Harms, M. C. Holthausen, J. Sundermeyer, S. Schindler, *Angew. Chem.* **2006**, *118*, 3951–3954; *Angew. Chem. Int. Ed.* **2006**, *45*, 3867–3869; c) C. J. Cramer, W. B. Tolman, *Acc. Chem. Res.* **2007**, *40*, 601–608; d) S. Yao, E. Bill, C. Milsmann, K. Wieghardt, M. Driess, *Angew. Chem.* **2008**, *120*, 7218–7221; *Angew. Chem. Int. Ed.* **2008**, *47*, 7110–7113; e) S. Yao, M. Driess, *Acc. Chem. Res.* **2012**, *45*, 276–287; f) I. Garcia-Bosch, X. Ribas, M. Costas, *Eur. J. Inorg. Chem.* **2012**, 179–187; g) R. Sarangi, *Coord. Chem. Rev.* **2013**, *257*, 459–472.

[3] a) L. Hammarstrom, S. Hammes-Schiffer, *Acc. Chem. Res.* **2009**, *42*, 1859–1860, and review articles in the special issue; b) K. Barnese, E. B. Gralla, D. E. Cabelli, J. S. Valentine, *J. Am. Chem. Soc.* **2008**, *130*, 4604–4606; c) R. Tagore, H. Chen, R. H. Crabtree, G. W. Brudvig, *J. Am. Chem. Soc.* **2006**, *128*, 9457–9465 and references therein; d) A. J. Wu, J. E. Penner-Hahn, V. L. Pecoraro, *Chem. Rev.* **2004**, *104*, 903–938.

[4] a) R. A. Geiger, S. Chattopadhyay, V. W. Day, T. A. Jackson, *J. Am. Chem. Soc.* **2010**, *132*, 2821–2831; b) R. L. Shook, A. S. Borovik, *Inorg. Chem.* **2010**, *49*, 3646–3660; c) S. Groni, P. Dorlet, G. Blain, S. Bourcier, R. Guillot, E. Anxolabéhère-Mallart, *Inorg. Chem.* **2008**, *47*, 3166–3172; d) R. L. Shook, W. A. Gunderson, J. Greaves, J. W. Ziller, M. P. Hendrich, A. S. Borovik, *J. Am. Chem. Soc.* **2008**, *130*, 8888–8889; e) S. Groni, G. Blain, R. Guillot, C. Policar, E. Anxolabéhère-Mallart, *Inorg. Chem.* **2007**, *46*, 1951–1953; f) N. Kitajima, H. Komatsuzaki, S. Hikichi, M. Osawa, Y. Moro-Oka, *J. Am. Chem. Soc.* **1994**, *116*, 11596–11597.

[5] a) Y. Hitomi, A. Ando, H. Matsui, T. Ito, T. Tanaka, S. Ogo, T. Funabiki, *Inorg. Chem.* **2005**, *44*, 3473–3478; b) R. Manchanda, G. W. Brudvig, R. H. Crabtree, *Coord. Chem. Rev.* **1995**, *144*, 1–38.

[6] Abbreviations of ligands used: 12-TMC = 1,4,7,10-tetramethyl-1,4,7,10-tetraazacyclododecane, 13-TMC = 1,4,7,10-tetramethyl-1,4,7,10-tetraazacyclotridecane, and 14-TMC = 1,4,8,11-tetramethyl-1,4,8,11-tetraazacyclotetradecane.

[7] a) J. Annaraj, J. Cho, Y.-M. Lee, S. Y. Kim, R. Latifi, S. P. de Visser, W. Nam, *Angew. Chem.* **2009**, *121*, 4214–4217; *Angew. Chem. Int. Ed.* **2009**, *48*, 4150–4153; b) M. S. Seo, J. Y. Kim, J. Annaraj, Y. Kim, Y.-M. Lee, S.-J. Kim, J. Kim, W. Nam, *Angew. Chem.* **2007**, *119*, 381–384; *Angew. Chem. Int. Ed.* **2007**, *46*, 377–380.

[8] J. Cho, R. Sarangi, W. Nam, *Acc. Chem. Res.* **2012**, *45*, 1321–1330.

[9] J. Cho, H. Kang, L. V. Liu, R. Sarangi, E. I. Solomon, W. Nam, *Chem. Sci.* **2013**, *4*, 1502–1508.

[10] W. Kohn, L. Sham, *J. Phys. Rev.* **1965**, *140*, A1133–A1138.

[11] R. A. Geiger, D. F. Leto, S. Chattopadhyay, P. Dorlet, E. Anxolabéhère-Mallart, T. A. Jackson, *Inorg. Chem.* **2011**, *50*, 10190–10203.

[12] C. J. Cramer, W. B. Tolman, K. H. Theopold, A. L. Rheingold, *Proc. Natl. Acad. Sci. USA* **2003**, *100*, 3635–3640.

[13] a) J. Cho, S. Jeon, S. A. Wilson, L. V. Liu, E. A. Kang, J. J. Braymer, M. H. Lim, B. Hedman, K. O. Hodgson, J. S. Valentine, E. I. Solomon, W. Nam, *Nature* **2011**, *478*, 502–505; b) J. Cho, R. Sarangi, H. Y. Kang, J. Y. Lee, M. Kubo, T. Ogura, E. I. Solomon, W. Nam, *J. Am. Chem. Soc.* **2010**, *132*, 16977–16986; c) J. Cho, R. Sarangi, J. Annaraj, S. Y. Kim, M. Kubo, T. Ogura, E. I. Solomon, W. Nam, *Nat. Chem.* **2009**, *1*, 568–572; d) A. Yokoyama, J. E. Han, J. Cho, M. Kubo, T. Ogura, M. A. Siegler, K. D. Karlin, W. Nam, *J. Am. Chem. Soc.* **2012**, *134*, 15269–15272.

[14] We have observed the formation of **2** and **3** in the range of 1–30 mM of **1**, and the amounts of the intermediates formed varied depending on the concentration of **1**.

[15] Although we are sure that the topology of the complex in Figure 2b is substantially correct, the poor quality of the structure due to disorder leads us to hesitate to discuss bond lengths and angles in detail.

[16] a) P. A. Goodson, A. R. Oki, J. Glerup, D. J. Hodgson, *J. Am. Chem. Soc.* **1990**, *112*, 6248–6254; b) J. Glerup, P. A. Goodson, A. Hazell, D. J. Hodson, C. J. McKenzie, K. Michelsen, U. Rychlewska, H. Toftund, *Inorg. Chem.* **1994**, *33*, 4105–4111.

[17] a) K. Honda, J. Cho, T. Matsumoto, J. Roh, H. Furutachi, T. Tosha, M. Kubo, S. Fujinami, T. Ogura, T. Kitagawa, M. Suzuki, *Angew. Chem.* **2009**, *121*, 3354–3357; *Angew. Chem. Int. Ed.* **2009**, *48*, 3304–3307; b) S. Itoh, H. Bandoh, M. Nakagawa, S. Nagatomo, T. Kitagawa, K. D. Karlin, S. Fukuzumi, *J. Am. Chem. Soc.* **2001**, *123*, 11168–11178; c) S. Hikichi, M. Yoshizawa, Y. Sasakura, M. Akita, Y. Moro-oka, *J. Am. Chem. Soc.* **1998**, *120*, 10567–10568; d) J. Cho, H. Furutachi, S. Fujinami, H. Ohtsu, T. Tosha, O. Ikeda, A. Suzuki, M. Nomura, T. Uruga, H. Tanida, T. Kawai, K. Tanaka, T. Kitagawa, M. Suzuki, *Inorg. Chem.* **2006**, *45*, 2873–2885.

[18] a) M. Suzuki, *Acc. Chem. Res.* **2007**, *40*, 609–617; b) M. J. Henson, P. Mukherjee, D. E. Root, T. D. P. Stack, E. I. Solomon, *J. Am. Chem. Soc.* **1999**, *121*, 10332–10345; c) P. L. Holland, C. J. Cramer, E. C. Wilkinson, S. Mahapatra, K. R. Rodgers, S. Itoh, M. Taki, S. Fukuzumi, L. Que, Jr., W. B. Tolman, *J. Am. Chem. Soc.* **2000**, *122*, 792–802.

[19] N. Kitajima, U. P. Singh, H. Amagai, M. Osawa, Y. Moro-oka, *J. Am. Chem. Soc.* **1991**, *113*, 7757–7758.

[20] References for the reactivities of $M(\mu\text{-}O)_2M$ (or M′) complexes in electrophilic and nucleophilic reactions: a) S. Kundu, F. F. Pfaff, E. Miceli, I. Zaharieva, C. Herwig, S. Yao, E. R. Farquhar, U. Kuhlmann, E. Bill, P. Hildebrandt, H. Dau, M. Driess, C. Limberg, K. Ray, *Angew. Chem.* **2013**, *125*, 5732–5736; *Angew. Chem. Int. Ed.* **2013**, *52*, 5622–5626; b) M. T. Kieber-Emmons, C. G. Riordan, *Acc. Chem. Res.* **2007**, *40*, 618–625.

[21] *Purification of Laboratory Chemicals* (Eds.: W. L. F. Armarego, D. D. Perrin), Pergamon, Oxford, **1997**.

[22] J. A. Halfen, V. G. Young, Jr., *Chem. Commun.* **2003**, 2894–2895.

[23] G. M. Sheldrick, SHELXTL/PC, Version 6.12 for Windows XP, **2001**, Bruker AXS Inc., Madison, Wisconsin, USA.
[24] a) A. D. Becke, *Phys. Rev. A* **1988**, *38*, 3098–3100; b) J. P. Perdew, *Phys. Rev. B* **1986**, *33*, 8822–8824.
[25] A. Schäfer, C. Huber, R. Ahlrichs, *J. Chem. Phys.* **1994**, *100*, 5829–5835.
[26] F. Neese, *WIREs Comput. Mol. Sci.* **2012**, *2*, 73–78.
[27] a) The ORCA basis set "CoreProp" was used. This basis is based on the TurboMole DZ basis developed by Ahlrichs and co-workers and obtained from the basis set library under ftp.chemie.uni-karlsruhe.de/pub/basen; b) F. Neese, *Inorg. Chim. Acta* **2002**, *337*, 181–192.
[28] S. Sinnecker, A. Rajendran, A. Klamt, M. Diedenhofen, F. Neese, *J. Phys. Chem. A* **2006**, *110*, 2235–2245.
[29] W. Humphrey, A. Dalke, K. Schulten, *J. Molec. Graphics.* **1996**, *14*, 33–38.

Received: April 29, 2013
Published online: August 16, 2013

